npj Climate and Atmospheric Science https://doi.org/10.1038/s41612-025-01306-3

Article in Press

A structural correction to atmospheric evaporative demand narrows the gap between offline aridity diagnostics and Earth system model projections

Received: 13 August 2025

Accepted: 19 December 2025

[redacted]

Cite this article as: Kim, D., Choi, M. A structural correction to atmospheric evaporative demand narrows the gap between offline aridity diagnostics and Earth system model projections. *npj Clim Atmos Sci* (2025). https://doi.org/10.1038/s41612-025-01306-3

Daeha Kim & Minha Choi

We are providing an unedited version of this manuscript to give early access to its findings. Before final publication, the manuscript will undergo further editing. Please note there may be errors present which affect the content, and all legal disclaimers apply.

If this paper is publishing under a Transparent Peer Review model then Peer Review reports will publish with the final article.

ARTICLE IN PRESS

© The Author(s) 2025. **Open Access** This article is licensed under a Creative Commons Attribution-NonCommercial-NoDerivatives 4.0 International License, which permits any non-commercial use, sharing, distribution and reproduction in any medium or format, as long as you give appropriate credit to the original author(s) and the source, provide a link to the Creative Commons licence, and indicate if you modified the licensed material. You do not have permission under this licence to share adapted material derived from this article or parts of it. The images or other third party material in this article are included in the article's Creative Commons licence, unless indicated otherwise in a credit line to the material. If material is not included in the article's Creative Commons licence and your intended use is not permitted by statutory regulation or exceeds the permitted use, you will need to obtain permission directly from the copyright holder. To view a copy of this licence, visit http://creativecommons.org/licenses/by-nc-nd/4.0/.

A structural correction to atmospheric evaporative demand narrows the gap between offline aridity diagnostics and Earth system model projections

Daeha Kim[1] and Minha Choi[2,3*]

[1]Department of Civil Engineering, Jeonbuk National University, Jeonbuk State, 54896, Republic of Korea

[2]School of Civil, Architectural Engineering & Landscape Architecture, Sungkyunkwan University, Suwon 16419, Republic of Korea

[3]Department of Global Smart City, Sungkyunkwan University, Suwon 16419, Republic of Korea

[*]Correspondence to: mhchoi@skku.edu

Abstract

Offline aridity and drought diagnostics typically project widespread terrestrial drying under climate change, whereas fully coupled Earth system models (ESMs) often simulate modest or regionally heterogeneous changes—and in some regions increasing—runoff. This long-standing divergence has been attributed largely to missing vegetation physiological effects and the neglect of sub-annual climate variability in offline diagnostic frameworks. Here we show that a more fundamental issue is the violation of the diagnostic framework's structural requirement that potential evapotranspiration (PET) and precipitation (P) act as independent climatic constraints. Using Penman and Penman–Monteith formulations, each with and without thermodynamic deflation via the complementary evaporation principle (CEP), we demonstrate that land–atmosphere feedbacks embedded in conventional PET estimates induce strong negative P–PET correlations (−0.45 ± 0.29; mean ± standard deviation) across land surfaces, which collapse toward near zero (−0.02 ± 0.42) after CEP deflation. Preserving PET–P independence substantially reduces inflation of the aridity index and brings offline diagnostic ET trends closer to ESM projections under a strong-emission scenario (from +0.61 to +0.39 mm yr^{-2}; ESM mean: +0.28 mm yr^{-2}). These results indicate that structural inconsistencies—rather than missing physiological processes alone—play a central role in the mismatch between offline diagnostics and ESM hydrology. Ensuring that PET is not inflated by land–atmosphere feedbacks is therefore essential for theoretically valid offline hydrologic assessments under a warming climate.

Keywords: Land–atmosphere feedbacks, Atmospheric evaporative demand, Budyko framework, Aridity index, Complementary evaporation principle

Introduction

Since the late 2010s, a persistent and unresolved question in hydrologic and climate-change sciences has been why runoff projections from Earth system models (ESMs) diverge from the signals implied by offline aridity and drought diagnostics[1–6]. Whereas ESMs simulate hydrological responses through fully coupled soil–vegetation–atmosphere interactions, offline indices typically combine precipitation (P) with an estimate of atmospheric evaporative demand—commonly expressed as potential evapotranspiration (PET)—to diagnose long-term water availability. These two approaches often yield contrasting interpretations: ESMs tend to project relatively modest or spatially heterogeneous changes in runoff, whereas offline metrics—especially those based on Penman-type or temperature-driven PET formulations—frequently suggest widespread and intensifying terrestrial drying[5–11].

This discrepancy has been commonly attributed to several factors. First, vegetation responds physiologically to both elevated atmospheric CO_2 concentration ($[CO_2]$) and rising dryness—often quantified using vapor pressure deficit (VPD)—by reducing stomatal conductance[12–14]. These reductions suppress actual evapotranspiration (ET), while PET continues to rise in most climate projections, causing aridity-based frameworks to overestimate land-surface drying and predict excessive declines in runoff[3,4,15]. Second, structural simplifications in the offline indices—such as their reliance on mean-state variables—overlook sub-annual variability (e.g., rainfall intermittency and seasonal distributions), which strongly shapes surface water balances[2]. Third, vegetation–climate feedbacks can influence not only ET but also P itself through changes in boundary-layer structure and convection. This further complicates the interpretation of drying trends in offline frameworks[16].

Although disabling physiological and variability-related processes in ESMs brings their behavior closer to offline diagnostics, it does not fully eliminate the divergence between the two approaches[2,17]. This persistent mismatch suggests that deeper structural issues remain unaddressed. Notably, offline diagnostic frameworks that use the aridity index (Φ = PET/P) to estimate ET or runoff—including Budyko-type equations[18]—implicitly assume that P and PET represent water supply and atmospheric demand independently.

The Budyko framework provides a simple yet widely used way to describe catchment-scale water balance by relating the ET ratio (ET/P) to Φ. In this framework, long-term mean ET is constrained by two independent climatic limits (i.e., P and PET) with catchment characteristics summarized by one or a small number of parameters[18]. Classical and modern formulations, including the perturbation analyses[19], therefore treat P, PET, and land-surface properties as separate, non-interacting drivers of ET. This structural independence assumption is central to the analytical convenience of Budyko-type models[20]. However, it has rarely been validated and is often violated in practice, especially when PET is derived from atmospheric variables that themselves respond to soil-moisture and land-surface conditions[21–23]. As a result, violations of the independence assumption can propagate through Φ-based diagnostics and lead to biased estimates of drying and runoff changes under a warming climate. Correcting the evaporative demand to reduce its dependence on P has been shown to significantly alter the runoff sensitivity to climatic and land-surface controls[24], underscoring the importance of preserving the theoretical assumptions built into Budyko-type models.

Still, it remains unclear whether the primary sources of divergence between Φ-based estimates and ESM-simulated ET stem from the omission of key physiological and land–atmosphere feedback processes or from limitations of the offline diagnostic framework itself. By correcting PET to account for both physiological responses and atmospheric feedbacks, we can assess how much of the gap between offline and ESM-based hydrologic estimates can be closed and thereby quantify the relative contributions of structural versus process-based deficiencies.

Results

Structural corrections to evaporative demand

In Budyko-type equations, atmospheric evaporative demand is conceptually defined as the "possible maximum ET" that would occur under prevailing climate conditions in the absence of surface moisture limitation[25]. A common approach to estimating this hypothetical amount is the open-water Penman equation[26], which combines two physical perspectives: an aerodynamic control, representing vapor removal by turbulent exchange; and a radiative control, representing the conversion of available net radiation into latent heat flux. However, its derivation implicitly assumes a uniformly wet, non-vegetated surface with fixed aerodynamic properties and no stomatal regulation. This represents an idealized upper bound that is unlikely to be realizable over vegetated land surfaces, where canopy structure, roughness length, and plant physiology can modify energy and vapor exchange[27].

Most land surfaces are at least partially vegetated with plants capable of accessing subsurface moisture and regulating water fluxes through stomatal conductance. The conventional Penman–Monteith formulation expands Penman's energy–aerodynamic combination by including a surface (canopy) resistance term, but its practical use has been limited by the difficulty of generalizing canopy-scale conductance[28,29]. Motivated by the discrepancies between offline projections and ESM hydrology, Yang et al. (ref.[3]) introduced a generic linear representation of stomatal closure under elevated [CO_2], and Liu et al. (ref.[15]) further embedded an optimal stomatal model[30] into the Penman–Monteith equation to explicitly represent the coupled effects of [CO_2], VPD, and leaf area index (LAI) on canopy conductance. Building on these developments, a two-source framework partitions PET into soil and vegetation components to better capture spatial heterogeneity in roughness and physiological controls[31]. Together, these advances demonstrate that conventional PET formulations tends to overestimate evaporative demand under warming, because it ignores physiological suppression of transpiration and the dynamic nature of canopy structure. Vegetation-responsive PET models thus provide a more physically consistent basis for estimating atmospheric demand over real land surfaces, although they remain influenced by atmospheric feedbacks when PET is driven directly by uncorrected atmospheric variables (temperature and VPD).

When the open-water Penman and vegetation-responsive Penman–Monteith formulations are forced with ERA5[32] atmospheric inputs, the resulting PET estimates—hereafter PET_{OW} and PET_{Veg} for open-water and vegetated cases, respectively—are frequently inflated over water-limited surfaces (Fig. 1). Under dry conditions, suppressed latent heat flux shifts the surface-energy balance toward sensible heating, raising near-surface air temperature and VPD[33]. This land–atmosphere feedback is widely documented by surface observations and theoretical frameworks for unsaturated landscapes[34–37]. Conversely, thermal imaging confirms that the surface temperatures over extensive saturated areas remain nearly constant with increasing distance from moisture discontinuities[38]. Thus, if the land surface were hypothetically saturated—as implied by the definition of possible maximum ET—the feedback-driven inflation would disappear, resulting in lower temperature and VPD. This “wet-surface reversal” underpins the complementary-evaporation principle (CEP)[21,22], which partially restores the Budyko assumption that PET is analytically independent of P (Methods).

The CEP framework provides a thermodynamic adjustment that deflates PET in both formulations—hereafter WET_{OW} and WET_{Veg} (Fig. 1d–e). Across water-limited areas, this deflation is larger than the PET reduction achieved when only [CO_2]- and VPD-driven stomatal responses are applied (Fig. 1c,g). Because CEP lowers VPD over a hypothetically saturated surface, the associated decline in stomatal conductance is smaller; with less physiological stress, transpiration does not need to be suppressed to the same extent (Fig. 1f).

The correlation maps between PET and P reveal that land–atmosphere feedbacks embed a pronounced dependence of evaporative demands on water supply across much of the globe (Fig. 2a–b). After applying the CEP correction, these correlations weaken noticeably—or even reverse in some regions—for the deflated estimates WET_{OW} and WET_{Veg} (Fig. 2d–e). Residual negative correlations likely arise from a purely radiative pathway: wetter years tend to be cloudier, reducing incoming short-wave radiation and thus lowering PET. Conversely, the positive correlations that appear over several (semi-)arid regions may reflect cases where higher warm-season surface radiation promotes boundary-layer instability and convective rainfall, consistent with the mechanism described by Seneviratne et al. (ref[39]). Globally, the Pearson correlation between P and the uncorrected PET averages -0.45 ± 0.29 (mean ± standard deviation) for PET_{OW} and -0.34 ± 0.29 for PET_{Veg}. After CEP deflation, these values shift substantially toward zero— -0.14 ± 0.42 for WET_{OW} and -0.02 ± 0.42 for WET_{Veg}—indicating that CEP mitigates much of the spurious P–PET coupling and moves the estimates closer to the Budyko framework’s requirement.

Historical trends of Φ and offline ET estimates

Over 1981–2020, the global annual Φ based on uncorrected PET ($\Phi_{P\text{-}OW}$ and $\Phi_{P\text{-}Veg}$) has risen significantly faster than its CEP-deflated counterpart ($\Phi_{W\text{-}OW}$ and $\Phi_{W\text{-}Veg}$) (Fig. 3a). By lowering the climatological mean of Φ and reducing its long-term slope, the CEP adjustment highlights how land–atmosphere feedbacks embedded in PET formulations can overstate the rate of surface drying. Because land–atmosphere coupling is projected to intensify under continued warming[40,41], $\Phi_{\text{P-OW}}$ values are likely to experience progressively larger inflation. Imposing stomatal constraints ($\Phi_{\text{P-Veg}}$)—representing reduced conductance under elevated [CO_2] and higher VPD—significantly moderates the inflated trend in $\Phi_{\text{P-OW}}$ ($p < 0.05$). Applying CEP deflation ($\Phi_{\text{W-OW}}$, $\Phi_{\text{W-Veg}}$) further dampens this trend ($p < 0.05$). After CEP is applied, however, additional stomatal adjustments exert insignificant influence on the trend ($p > 0.3$), because the hypothetically saturated surface implicitly maintains a low VPD, leaving little room for further physiological suppression.

Despite their significantly different trends, all four Φ series allow a commonly used Budyko-type model to reproduce ERA5's long-term ET trajectory with comparable accuracy (Fig. 3b). The Turc–Mezentsev equation[42] is a frequently used parametric function that converts Φ into the ET ratio through a single land-specific exponent *n* (Methods). For each Φ series, we calibrate the exponent *n* on a pixel-by-pixel basis to match the 1985–2014 climatological mean ET (Supplementary Fig. S1). The resulting *n* values exhibit a clear breakpoint at $\Phi_0 \approx 1$ in log–log space (Supplementary Fig. S2). For $\Phi < \Phi_0$ (i.e., P > PET), surplus P produces saturation-excess overland flow while ET remains capped at PET, driving *n* downward with decreasing Φ[24]. Conversely, for $\Phi > \Phi_0$, *n* correlates negatively with Φ, reflecting dominant infiltration-excess overland flow in drier climates[43], which diverts water to runoff and reduces the ET ratio.

Assuming a quasi–steady state, we then simulate annual ET for 1981–2020 by applying each Φ series—with its calibrated *n*—to the Turc–Mezentsev equation. Here, *n* is allowed to vary each year according to its statistical sensitivity to changes in Φ. When these simulations are compared against ERA5's annual ET (independent of the calibration period), predictive performance slightly improves as we move from uncorrected to CEP-deflated PET formulations (Supplementary Fig. S3). The anomaly correlations between ERA5's global mean ET and the Φ-based predictions are 0.81 for $\Phi_{\text{P-OW}}$, 0.78 for $\Phi_{\text{P-Veg}}$, 0.84 for $\Phi_{\text{W-OW}}$, and 0.79 for $\Phi_{\text{W-Veg}}$. Across land surfaces, the mean biases of the simulated ET anomalies range from 2.9 ± 28 mm yr^{-1} ($\Phi_{\text{P-OW}}$) and 4.3 ± 27 mm yr^{-1} ($\Phi_{\text{P-Veg}}$) to 1.7 ± 25 mm yr^{-1} ($\Phi_{\text{W-OW}}$) and 3.4 ± 25 mm yr^{-1} ($\Phi_{\text{W-Veg}}$), indicating that CEP deflation systematically reduces ET anomaly biases, whereas incorporating physiological responses alone yields little additional improvement.

Nonetheless, all four simulated ET series exhibit statistically indistinguishable long-term trends ($p > 0.35$), suggesting that the choice of PET formulation has little impact on reconstructing historical ET trends. This similarity arises because land–atmosphere feedback effects are implicitly absorbed into the calibrated exponent *n* for each formulation. However, as climate conditions increasingly diverge from historical patterns, the influence of feedbacks inherent in the uncorrected PET estimates, when compared with the CEP-deflated WET estimates, becomes progressively more evident.

Global ET trends under a warming scenario: Budyko diagnostics vs. ESM projections

Figure 4 compares century-scale trajectories of both Φ and resulting ET anomalies from four Budyko-based formulations against the multi-model mean of ten Coupled Model Intercomparison Project Phase 6 (CMIP6)[44] model projections (Table S1) under the business-as-usual Shared Socioeconomic Pathway (SSP) 5-8.5 scenario[45]. For the late-century period (2071–2100), correlations between P and the uncorrected PET estimates (PET_{OW}, PET_{Veg}) remains high, but they weaken markedly once CEP deflation is applied (WET_{OW}, WET_{Veg}), consistent with the historical behavior (Supplementary Fig. S4). Notably, the decline in P–PET_{Veg} correlation is even more pronounced than in the ERA5 analysis, implying that the physiological influence strengthens as warming and VPD intensify.

The Turc–Mezentsev equation continues to reproduce ESM-simulated ET reasonably well, with modest improvement from CEP deflation (Supplementary Fig. S5). The smaller gain in $\mathrm{WET_{Veg}}$ relative to $\mathrm{WET_{OW}}$ likely reflects the deep uncertainty in representing physiological responses within evaporative-demand formulations (ref.[46]). Nonetheless, both CEP-deflated estimates improve Budyko–ESM agreement more in 2071–2100 than in the ERA5 analysis, due partly to amplified feedback-driven inflation under future warming. Across land surfaces for 2071–2100, the ensemble-mean biases of Budyko-derived ET anomalies are 35.0 ± 46.5 mm $\mathrm{yr^{-1}}$ for $\mathrm{PET_{OW}}$ and 18.5 ± 42.0 mm $\mathrm{yr^{-1}}$ for $\mathrm{PET_{Veg}}$, decreasing to 21.0 ± 35.7 mm $\mathrm{yr^{-1}}$ for $\mathrm{WET_{OW}}$ and 10.1 ± 38.3 mm $\mathrm{yr^{-1}}$ for $\mathrm{WET_{Veg}}$. These reductions indicate that both CEP deflation and physiological adjustments play increasingly important roles in improving hydrologic consistency under late-century climate conditions.

In Fig. 4a, all four Φ anomaly series fluctuate near zero during 1985–2014 before diverging sharply after 2020. The uncorrected open-water formulation ($\Phi_{\mathrm{P\text{-}OW}}$) exhibits the steepest rise (+0.10 % $\mathrm{yr^{-1}}$), followed by the uncorrected vegetated version ($\Phi_{\mathrm{P\text{-}Veg}}$; +0.05 % $\mathrm{yr^{-1}}$). Applying CEP deflation alone ($\Phi_{\mathrm{W\text{-}OW}}$; +0.05 % $\mathrm{yr^{-1}}$) and combining it with physiological suppression ($\Phi_{\mathrm{W\text{-}Veg}}$; +0.02 % $\mathrm{yr^{-1}}$) progressively flattens the trend. Although $\Phi_{\mathrm{P\text{-}Veg}}$ increases more rapidly than $\Phi_{\mathrm{W\text{-}OW}}$ in the ERA5-based analysis (where LAI held fixed), dynamic vegetation changes in ESMs—particularly to rising LAI under elevated [$\mathrm{CO_2}$]—likely moderate the $\Phi_{\mathrm{P\text{-}Veg}}$ projection under SSP5-8.5.

In Fig. 4b, the linear trends of ET anomalies derived from all four Φ formulations appear to be indistinguishable through the historical period (1980–2014), reconfirming that the choice of

PET formulation has minimal impact on reconstructing past ET trends. Under SSP5-8.5 by 2100, however, the uncorrected PET_{OW} produces a trend of +0.61 mm yr^{-2}—more than double the ESM ensemble mean of +0.28 mm yr^{-2} ($p < 0.001$). Applying either CEP deflation (WET_{OW}) or physiological suppression (PET_{Veg}) individually reduces the Budyko-derived trend to +0.48 mm yr^{-2}, bringing it closer to the ESM projections. Combining both corrections (WET_{Veg}) narrows the gap further to +0.39 mm yr^{-2}, although a significant overestimation remains ($p < 0.001$).

Discussion

Previous studies have primarily attributed the divergence between Φ-based diagnostics and ESM projections to missing process representations in PET—most notably, stomatal responses to elevated [CO_2] and VPD[3,12–15]—or to the use of mean-state climate metrics that overlook intra-annual variability[1,2,17,47]. Incorporating these physiological and variability-related processes may reduce the mismatch between offline diagnostics and ESM outputs, but such corrections would still treat PET as an externally imposed, empirically tuned demand term. Crucially, they do not resolve the deeper structural assumption underpinning Budyko-type frameworks: PET and P represent independent climatic constraints. When PET is computed directly from atmospheric variables such as temperature and VPD—which themselves respond to land-surface moisture conditions—this independence breaks down. Violations of this assumption introduce a structural inconsistency that persists even after physiological processes are incorporated and may be more fundamental than the missing processes themselves.

A recent study by Zhou & Yu (ref.[48]) provides independent support for this interpretation. They quantified PET using two physically distinct formulations—an energy-based PET (PET_e) and an aerodynamic PET (PET_a)—and demonstrated that the divergence between them ($PET_a > PET_e$) reflects land–atmosphere feedbacks arising from reduced ET. Because Penman-type PET combines both energy and aerodynamic controls, it inherits this feedback-driven inflation, leading to a 25–39% overestimation of climate-driven ET increases and a 77–121% exaggeration of land-surface suppression effects in Budyko-type analyses. When the physiological effects of elevated [CO_2] are disabled, Φ constructed with PET_e reproduces the ET changes simulated by ESMs, indicating that PET_e captures the pure radiative forcing of increasing [CO_2] without contamination from feedback-driven atmospheric drying. In contrast, our CEP method reconstructs the wet-surface state by thermodynamically reversing the observed warming and drying. Although the two approaches differ conceptually, both converge on the same conclusion: inflated PET in water-limited environments originates from land–atmosphere feedbacks, not from externally forced atmospheric drying.

In our analysis, the CEP-deflated PET fields (Fig. 1d–e) exhibit a pronounced latitudinal gradient that closely tracks net radiation patterns, as also reported by Zhou & Yu (ref.[48]), whereas uncorrected PET peaks in subtropical "horse-latitude" regions where feedback-driven inflation is strongest. Although PET inflation can accelerate local moisture loss and exacerbate plant stress[22,34,49], this inflation disappears when the surface is saturated at basin scales—clarifying why the Budyko framework's "possible maximum ET" is better represented by CEP-deflated than by uncorrected Penman-type estimates. Correcting this feedback-driven inflation is therefore essential for any theoretically valid application of Budyko-type models.

Moreover, the magnitude—and even the sign—of stomatal responses to elevated [CO_2] remains highly uncertain[46]. Meta–analyses and ESM intercomparisons reveal large variability across species, biomes, moisture regimes, and nutrient states, suggesting that reductions in stomatal conductance may only partially or transiently offset the warming-driven increases in PET. This physiological uncertainty, coupled with the structural limitations inherent to offline

PET formulations, further underscores that preserving the Budyko requirement of P–PET independence is more fundamental than embedding additional process-based adjustments into PET itself.

While Zhou & Yu (ref.[48]) demonstrate that the PET_e-based Budyko framework can successfully reproduce the radiative effects of elevated [CO_2], their formulation does not represent the physiological pathways through which [CO_2] alters stomatal conductance and transpiration, and thus cannot capture the combined radiative–physiological responses simulated in fully coupled ESMs. In contrast, our CEP approach incorporates an optimal-conductance model to approximate stomatal and canopy-scale physiological adjustments, though this representation remains imperfect and residual correlations between meteorological variables and ET cannot be fully eliminated. A limitation common to both studies is reliance on climatological, annual-mean relationships; sub-annual variability—which modulates subsurface storage dynamics—is not explicitly resolved. Together, these limitations point to the need for further development of offline frameworks that more fully capture both physiological responses and sub-annual processes represented in ESMs.

Relying solely on atmospheric variables to diagnose water balance and associate stresses becomes increasingly problematic under global warming, especially as terrestrial relative humidity continues to decline[50–52]. The conceptual link between atmospheric aridity and surface water balance is complicated not only by uncertain physiological adjustments, but—more importantly—by the theoretical misfit of conventional PET formulations in a warming climate. Although it does not completely eliminate the statistical coupling between P and PET, CEP-deflation substantially narrows the gap between offline aridity indices and ESM-simulated ET. We highlight that the persistent mismatch between offline diagnostics and ESM projections arises not only from missing processes in PET formulations, but from the fundamental theoretical limitations of conventional offline frameworks when their structural assumptions are violated.

Methods

Climate reanalysis, Earth system model projections, and [CO_2] data

We obtained monthly meteorological data from ERA5 (1980–2014) and ten CMIP6 ESMs (historical: 1980–2014; SSP5-8.5: 2015–2100; Supplementary Table 1). From ERA5, we used precipitation (P), actual evapotranspiration (ET), 2m air and dew-point temperatures (T_a, T_d), surface net radiation (R_n), given as the sum of latent and sensible heat fluxes, 2m wind speed (u)—converted from 10m values via a power-law profile—and LAI, all at 0.25°×0.25°. For CMIP6 models, VPD was calculated by relative humidity instead of T_d, with all other variables matched where available. Native CMIP6 outputs were bilinearly regridded to a common 1°×1° resolution and aggregated to annual values.

Vegetated PET estimates (PET_{Veg} and WET_{Veg}) require [CO_2] data. We employed the gridded datasets produced by Cheng et al. (ref.[53]). The historical records span from 1980 to 2013; the 2014 values were linearly interpolated, and 2015–2020 concentrations were taken as the mean of the SSP1-2.6 and SSP5-8.5 pathways, matching the observed global trend (Supplementary Fig. S6). For projections (2015–2100), the historical [CO_2] series was seamlessly extended with the SSP5-8.5 trajectory to maintain consistency with the CMIP6 forcing scenario.

Open-water Penman and two-source Penman-Montieth formulations

The Penman equation is a simplified water demand model assuming an open-water surface with a fixed aerodynamic roughness. Using R_n (J m^{-2} s^{-1}), T_a (K), T_d (K), and u (m s^{-1}), it computes PET (kg m^{-2} s^{-1}) as:

$$\mathrm{PET_{OW}} = \frac{sR_n + \gamma \frac{6.43(1+0.536u)}{8.64\times10^{7}} \mathrm{VPD}}{\lambda(s+\gamma)}, \tag{1}$$

where s is the slope of the saturation vapor-pressure curve (Pa K^{-1}), γ is the psychrometric constant (Pa K^{-1}), λ is the latent heat of vaporization (J kg^{-1}), and VPD is calculated as the difference between saturation vapor pressures at T_a and T_d (Pa). The factor 8.64×10^7 ensures that PET_{OW} is expressed in kg m^{-2} s^{-1}.

To capture heterogeneity of land surfaces, we employed the two-source Penman-Monteith approach[31], which partitions PET_{Veg} into vegetated and bare-soil components:

$$\mathrm{PET_{Veg}} = \mathrm{f_c E_{p,v}} + (1 - \mathrm{f_c})\mathrm{E_{p,s}}, \tag{2}$$

where $E_{p,v}$ and $E_{p,s}$ denote the vegetated and bare-soil components, and f_c is the vegetation cover fraction estimated using the Beer–Lambert law:

$$\mathrm{f_c} = 1 - \exp(-\mathrm{kLAI}\,), \tag{3}$$

with k = 0.56 representing a typical extinction coefficient[54].

Evaporative demand over each component ($E_{p,v}$ and $E_{p,s}$) is then computed using the Penman–Monteith equation:

$$\lambda \mathrm{E_p} = \frac{\mathrm{sR_n} + \rho_a \mathrm{C_p VPD}/\mathrm{r_a}}{\mathrm{s} + \gamma(1 + \mathrm{r_s}/\mathrm{r_a})}, \tag{4}$$

where ρ_a is air density (kg m^{-3}), C_p is the specific heat of air (J kg^{-1} K^{-1}), and r_a and r_s are the aerodynamic and surface resistances (s m^{-1}), respectively.

For the bare soil component, roughness lengths were set at 2.74 mm (momentum) and 0.177 mm (heat and vapor), with the zero-plane displacement considered negligible[55]. For the vegetated component, roughness lengths were estimated from empirical relationships with vegetation heights[56], where vegetation height h (m) was approximated as h = LAI/(f_c×24).

The two-source model neglects r_s for bare soil, while the vegetated component is assumed to be controlled by the optimal leaf-level conductance[30] ($g_{s,l}$) (mol m^{-2} s^{-1}) as:

$$\mathrm{g_{s,l}} = 1.6\left(1 + \frac{\mathrm{g_1}}{\mathrm{VPD}^{1/2}}\right)\frac{\mathrm{A}}{[\mathrm{CO_2}]}, \tag{5}$$

where g_1 is the marginal water-use efficiency parameter ($Pa^{1/2}$), A is the net assimilation rate (μmol m^{-2} s^{-1}), and [CO_2] is in ppm. Canopy-level conductance (g_s, mol m^{-2} s^{-1}) is then scaled from $g_{s,l}$ using the active portion of LAI: $g_s = g_{s,l}(0.5LAI/f_c)$, and r_s becomes the reciprocal of g_s. The associated parameters g_1 and A are determined by following the empirical relationships by Lin et al. (ref.[57]) established with climate conditions and assimilation sensitivity to changes in [CO_2].

Deflating PET by a graphical CEP framework

To remove land–atmosphere feedbacks embedded in conventional PET estimates, we applied the isenthalpic CEP framework of Crago & Qualls (ref.[21]). The CEP method reconstructs the air temperature (T_{PT}) and vapor pressure (e_{PT}) that would prevail over a saturated surface, thereby excluding the soil- or canopy-driven warming and VPD inflation that typically enhance PET over water-limited regions.

In the temperature–vapor-pressure [T, e] plane (Fig. S7), the ambient air state [T_a, e_a] lies on an air isoenthalp—a straight line with slope −γ along which all points share the same moist enthalpy. To satisfy the surface energy balance, a surface isoenthalp must run parallel to the air isoenthalp but be displaced rightward by a thermodynamic offset of $0.622R_n/[pC_pf(u)]$ (K), where p is atmospheric pressure (Pa) and f(u) is the wind function:

$$f(u) = \begin{cases} \frac{6.43(1+0.536u)}{8.64\times10^7} & \text{for } PET_{OW} \\ \frac{0.622}{R_d T_a r_a}, & \text{for } PET_{Veg} \end{cases}, \qquad (6)$$

with $R_d = 287$ J kg^{-1} K^{-1}. Every point on the surface isoenthalp represents a feasible combination of surface temperature and vapor pressure that converts R_n into turbulent heat fluxes. This line intersects the saturation vapor-pressure curve $e^*(T)$ at the wet-surface state [T_{ws}, $e^*(T_{ws})$], which corresponds to the equilibrium surface temperature expected if the surface were completely saturated.

Although air adjacent to a saturated surface is assumed to be saturated, the overlying boundary layer is typically subsaturated owing to advective entrainment[58]. To determine the air state that would exist over the hypothetically wet surface, a straight line with slope $s' = s\alpha\gamma/[s(1-\alpha) + \gamma]$ is drawn from $[T_{ws}, e^*(T_{ws})]$, where the Priestley–Taylor coefficient[59] is:

$$\alpha = \frac{s+\gamma}{s+0.55\gamma}. \tag{7}$$

For s', both s and α are evaluated at T_{ws}[22,60]. The intersection of this line with the original air isoenthalp yields the wet-environment air state $[T_{PT}, e_{PT}]$, representing the temperature and humidity that would occur above the saturated surface in the absence of land-surface drying.

Finally, substituting $[T_{PT}, e_{PT}]$ for $[T_a, e_a]$ in the open-water Penman and the two-source Penman–Monteith formulations—while retaining the given R_n and u—yields the CEP-deflated PET estimates, denoted WET_{OW} and WET_{Veg}.

Translating Φ into land-surface water balance

To convert the aridity index ($\Phi = PET/P$) into the ET ratio (ET/P), we employed the Turc–Mezentsev equation:

$$\frac{ET}{P} = \left[\frac{1}{1+\left(\frac{PET}{P}\right)^{-n}}\right]^{1/n}, \tag{8}$$

where the dimensionless exponent *n* summarizes catchment attributes (e.g., topography, soil texture, rooting depth, vegetation cover).

For every ERA5 and CMIP6 grid cell, we inverted Eq. (8) to obtain the baseline exponent (n_{clim})—the value that exactly reproduces the 1985–2014 mean ET ratio. Assuming negligible water storage changes, year-to-year departures of *n* from n_{clim} were allowed to track the sensitivity of *n* to changes in Φ. This sensitivity was quantified by fitting a piece-wise linear relationship in log-log space (Supplementary Fig. S3):

$$\ln \mathrm{n} = \begin{cases} \mathrm{a}_0 + \mathrm{a}_1 \ln \Phi & \text{for } \Phi \leq \Phi_0 \\ \mathrm{a}_0 + \mathrm{a}_2 \left(\ln \Phi - \ln \Phi_0\right) & \text{for } \Phi > \Phi_0 \end{cases}, \tag{9}$$

where Φ_0 is the break point between humid and arid regimes and (a_0, a_1, a_2) are regression coefficients. The same Φ–*n* regressions, calibrated separately for each of the ten ESMs (Supplementary Table S2), were then applied cell-by-cell to generate a time-varying exponent *n* that reflect annual shifts in Φ while preserving the 30-year climatological mean.

Annual water-balance estimates computed with by Eq. (8) using varying *n* remain tightly correlated with the CMIP6 models' explicit ET—maintaining high skill even in the late-century window (2071–2100)—while offering a computationally parsimonious alternative for tracing evaporative responses to evolving aridity.

Competing Interests

All authors declare no financial or non-financial competing interests.

Author contributions

D.K. conceived the study, performed the calculations, generated the visualizations, drafted the manuscript, and led the interpretation and discussion of the results. M.C. contributed to the discussion, interpretation, and revision of the manuscript. All authors reviewed and approved the final manuscript.

Data availability

The ERA5 reanalysis and CMIP6 datasets used to reproduce the results of this study are publicly available from the Copernicus Climate Data Store (https://cds.climate.copernicus.eu/) and the IPSL ESGF node (https://esgf-node.ipsl.upmc.fr/projects/cmip6-ipsl/), respectively. The downscaled [CO2] dataset is accessible at Zenodo (https://zenodo.org/records/5021361).

Code availability

Python scripts used to estimate PET from meteorological inputs and to apply the CEP deflation are available upon reasonable requests from the first author (daeha.kim@jbnu.ac.kr).

Acknowledgements

This work was supported by the National Research Foundation of Korea (NRF) grant funded by the Korea government (MSIT) (RS-2024-00416443).

References

1. Vicente-Serrano, S.M. et al. Atmospheric drought indices in future projections. Nat. Water 3, 374–387 (2025).
2. Scheff, J., Coats, S. & Laguë, M.M. Why do the global warming responses of land-surface models and climatic dryness metrics disagree?. Earths Future 10, e2022EF002814 (2022).
3. Yang, Y. et al. Hydrologic implications of vegetation response to elevated CO_2 in climate projections. Nat. Clim. Change 9, 44–48 (2019).
4. Milly, P. C. & Dunne, K.A. Potential evapotranspiration and continental drying. Nat. Clim. Change 6, 946–949 (2016).
5. Yang, Y. et al. Comparing Palmer Drought Severity Index drought assessments using the

traditional offline approach with direct climate model outputs. Hydrol. Earth Syst. Sci. 24, 2921–2930 (2020).

6. Kim, D., Chun, J.A., Yeo, J.H. & Ha, K.J. Divergent flash-drought risks indicated by evaporative stress and soil-moisture projections under warming scenarios. Environ. Res. Lett. 18, 094023 (2023).
7. Greve, P., Roderick, M.L., Ukkola, A.M. & Wada, Y. The aridity index under global warming. Environ. Res. Lett. 14, 124006 (2019).
8. Scheff, J. A unified wetting and drying theory. Nat. Clim. Change 9, 9–10 (2019).
9. Berg, A. & Sheffield, J. Climate change and drought: the soil-moisture perspective. Curr. Clim. Change Rep. 4, 180–191 (2018).
10. Milly, P. C. D. & Dunne, K. A. A hydrologic drying bias in water-resource impact analyses of anthropogenic climate change. J. Am. Water Resour. Assoc. 53, 822–838 (2017).
11. Roderick, M.L., Greve, P. & Farquhar, G.D. On the assessment of aridity with changes in atmospheric CO_2. Water Resour. Res. 51, 5450–5463 (2015).
12. Swann, A.L., Hoffman, F.M., Koven, C.D. & Randerson, J.T. Plant responses to increasing CO_2 reduce estimates of climate impacts on drought severity. Proc. Natl Acad. Sci. USA 113, 10019–10024 (2016).
13. Lemordant, L. et al. Critical impact of vegetation physiology on the continental hydrologic cycle in response to increasing CO_2. Proc. Natl Acad. Sci. USA 115, 4093–4098 (2018).
14. Scheff, J. Drought indices, drought impacts, CO_2, and warming: a historical and geologic perspective. Curr. Clim. Change Rep. 4, 202–209 (2018).
15. Liu, Z. et al. A physically based potential evapotranspiration model for global water-availability projections. J. Hydrol. 622, 129767 (2023).

16. Lesk, C.S., Winter, J.M. & Mankin, J.S. Projected runoff declines from plant physiological effects on precipitation. Nat. Water 3, 167–177 (2025).

17. Scheff, J., Mankin, J.S., Coats, S. & Liu, H. CO_2-plant effects do not account for the gap between dryness indices and projected dryness impacts in CMIP6 or CMIP5. Environ. Res. Lett. 16, 034018 (2021).

18. Mianabadi, A., Davary, K., Pourreza-Bilondi, M. & Coenders-Gerrits, A.M.J. Budyko framework: towards non-steady-state conditions. J. Hydrol. 588, 125089 (2020).

19. Roderick, M. L. & Farquhar, G. D. A simple framework for relating variations in runoff to variations in climatic conditions and catchment properties. Water Resour. Res. 47, W00G07 (2011).

20. Yang, H., Yang, D., Lei, Z. & Sun, F. New analytical derivation of the mean annual water-energy balance equation. Water Resour. Res. 44, W03410 (2008).

21. Crago, R.D. & Qualls, R.J. A graphical interpretation of the rescaled complementary relationship for evapotranspiration. Water Resour. Res. 57, e2020WR028299 (2021).

22. Szilagyi, J. On the thermodynamic foundations of the complementary relationship of evaporation. J. Hydrol. 593, 125916 (2021).

23. Han, S. & Tian, F. A review of the complementary principle of evaporation: from the original linear relationship to generalized nonlinear functions. Hydrol. Earth Syst. Sci. 24, 2269–2285 (2020).

24. Kim, D. & Chun, J.A. Revisiting a two-parameter Budyko equation with the complementary-evaporation principle for proper consideration of surface-energy balance. Water Resour. Res. 57, e2021WR030838 (2021).

25. Zhang, L., & Brutsaert, W. Blending the evaporation precipitation ratio with the

complementary principle function for the prediction of evaporation. Water Resour. Res. 57, e2021WR029729 (2020).

26. Penman, H.L. Natural evaporation from open water, bare soil and grass. Proc. R. Soc. Lond. A 193, 120–145 (1948).
27. Lhomme, J. P. Towards a rational definition of potential evaporation. Hydrol. Earth Syst. Sci. 1, 257–264 (1997).
28. Penman, H. L. Evaporation: an introductory survey. Neth. J. Agric. Sci. 4, 9–29 (1956).
29. Monteith, J. L. Evaporation and environment. Symp. Soc. Exp. Biol. 19, 205–234 (1965).
30. Medlyn, B. E. et al. Reconciling the optimal and empirical approaches to modelling stomatal conductance. Glob. Change Biol. 17, 2134–2144 (2011).
31. Kim, D., Choi, M. & Kang, M. Testing new potential-evaporation formulations for identifying soil-moisture deficiency in agricultural areas under global warming. J. Hydrol. 661, 133760 (2025).
32. Soci, C. et al. The ERA5 global reanalysis from 1940 to 2022. Q. J. R. Meteorol. Soc. 150, 4014–4048 (2024).
33. Gebrechorkos, S. H. et al. Warming accelerates global drought severity. Nature 642, 628–635 (2025).
34. Zhou, S. et al. Land–atmosphere feedbacks exacerbate concurrent soil drought and atmospheric aridity. Proc. Natl Acad. Sci. USA 116, 18848–18853 (2019).
35. Szilagyi, J. Temperature corrections in the Priestley–Taylor equation of evaporation. J. Hydrol. 519, 455–464 (2014).
36. Huntington, J. L., Szilagyi, J., Tyler, S.W. & Pohll, G. M. Evaluating the complementary relationship for estimating evapotranspiration from arid shrublands. Water Resour. Res. 47,

W05533 (2011).

37. Lobell, D. B. & Bonfils, C. The effect of irrigation on regional temperatures: A spatial and temporal analysis of trends in California, 1934–2002. J. Clim. 21, 2063–2071 (2008).
38. Szilagyi, J. & Schepers, A. Coupled heat and vapor transport: The thermostat effect of a freely evaporating land surface. Geophy. Res. Lett. 41, 435–441 (2014).
39. Seneviratne, S. I. et al. Investigating soil-moisture–climate interactions in a changing climate: a review. Earth-Sci. Rev. 99, 125–161 (2010).
40. Berg, A. et al. Land–atmosphere feedbacks amplify aridity increase over land under global warming. Nat. Clim. Change 6, 869–874 (2016).
41. Denissen, J.M. et al. Widespread shift from ecosystem energy to water limitation with climate change. Nat. Clim. Change 12, 677–684 (2022).
42. Andréassian, V. & Sari, T. On the puzzling similarity of two water-balance formulas—Turc–Mezentsev vs. Tixeront–Fu. Hydrol. Earth Syst. Sci. 23, 2339–2350 (2019).
43. Kidron, G. J. Comparing overland-flow processes between semiarid and humid regions: does saturation overland flow take place in semiarid regions? J. Hydrol. 593, 125624 (2021).
44. Eyring, V. et al. Overview of the Coupled Model Intercomparison Project Phase 6 (CMIP6) experimental design and organization. Geosci. Model Dev. 9, 1937–1958 (2016).
45. O'Neill, B.C. et al. The Scenario Model Intercomparison Project (ScenarioMIP) for CMIP6. Geosci. Model Dev. 9, 3461–3482 (2016).
46. Vicente-Serrano, S.M. et al. The uncertain role of rising atmospheric CO_2 on global plant transpiration. Earth-Sci. Rev. 230, 104055 (2022).
47. Zaitchik, B.F., Rodell, M., Biasutti, M. & Seneviratne, S.I. Wetting and drying trends under climate change. Nat. Water 1, 502–513 (2023).

48. Zhou, S. & Yu, B. Neglecting land–atmosphere feedbacks overestimates climate-driven increases in evapotranspiration. Nat. Clim. Change, 1099–1106 (2025).
49. Lesk, C. et al. Stronger temperature–moisture couplings exacerbate the impact of climate warming on global crop yields. Nat. Food 2, 683–691 (2021).
50. Douville, H. et al. Drivers of the enhanced decline of land near-surface relative humidity to abrupt 4×CO_2 in CNRM-CM6-1. Clim. Dyn. 55, 1613–1629 (2020).
51. Byrne, M. P. & O'Gorman, P.A. Understanding decreases in land relative humidity with global warming: conceptual model and GCM simulations. J. Clim. 29, 9045–9061 (2016).
52. Huang, J., Yu, H., Guan, X., Wang, G. & Guo, R. Accelerated dryland expansion under climate change. Nat. Clim. Change 6, 166–171 (2016).
53. Cheng, W. et al. Global monthly gridded atmospheric carbon-dioxide concentrations under historical and future scenarios. Sci. Data 9, 83 (2022).
54. Zhang, L., Hu, Z., Fan, J., Zhou, D. & Tang, F. A meta-analysis of the canopy light extinction coefficient in terrestrial ecosystems. Fron. Earth Sci. 8, 599–609 (2014).
55. Yang, K. et al., Turbulent flux transfer over bare-soil surfaces: Characteristics and parameterization. J. Appl. Meteorol. Climatol. 47, 276–290 (2008).
56. Allen, R.G., Pereira, L.S., Raes, D. & Smith, M. Crop Evapotranspiration (guidelines for computing crop water requirements). FAO Irrigation and drainage paper No. 56. Food and Agriculture Organization of the United Nations, Rome, Italy (1998).
57. Lin, Y. S. et al. Optimal stomatal behaviour around the world. Nat. Clim. Change 5, 459–464 (2015).
58. Brutsaert, W., & Stricker, H. An advection-aridity approach to estimate actual regional evapotranspiration. Water Resour. Res. 15, 443–450 (1979).

59. Priestley, C. H. B. & Taylor, R. J. On the assessment of surface heat flux and evaporation using large-scale parameters. Mon. Weather Rev. 100, 81–92 (1972).

60. Szilagyi, J. & Crago, R. D. A thermodynamics-based versatile evapotranspiration-estimation method of minimum data requirement for water-resources investigations. J. Hydrol. 624, 129917 (2023).

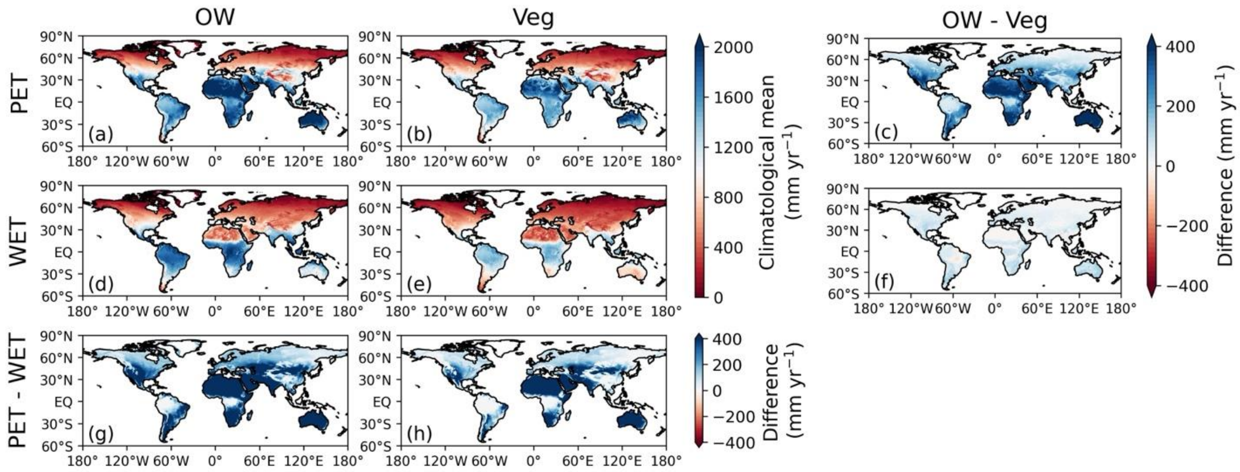

Fig. 1 Spatial distributions of climatological (1985–2014) evaporative demand estimates and their pairwise differences. **a**,**b**, Mean annual PET$_{\mathrm{OW}}$ and PET$_{\mathrm{Veg}}$, respectively. **c**, PET$_{\mathrm{OW}}$ minus PET$_{\mathrm{Veg}}$. **d,e**, Mean annual WET$_{\mathrm{OW}}$ and WET$_{\mathrm{Veg}}$, respectively **f**, WET$_{\mathrm{OW}}$ minus WET$_{\mathrm{Veg}}$. **g,h**, Feedback-driven inflations: PET$_{\mathrm{OW}}$ – WET$_{\mathrm{OW}}$ (g) and PET$_{\mathrm{Veg}}$ – WET$_{\mathrm{Veg}}$ (h).

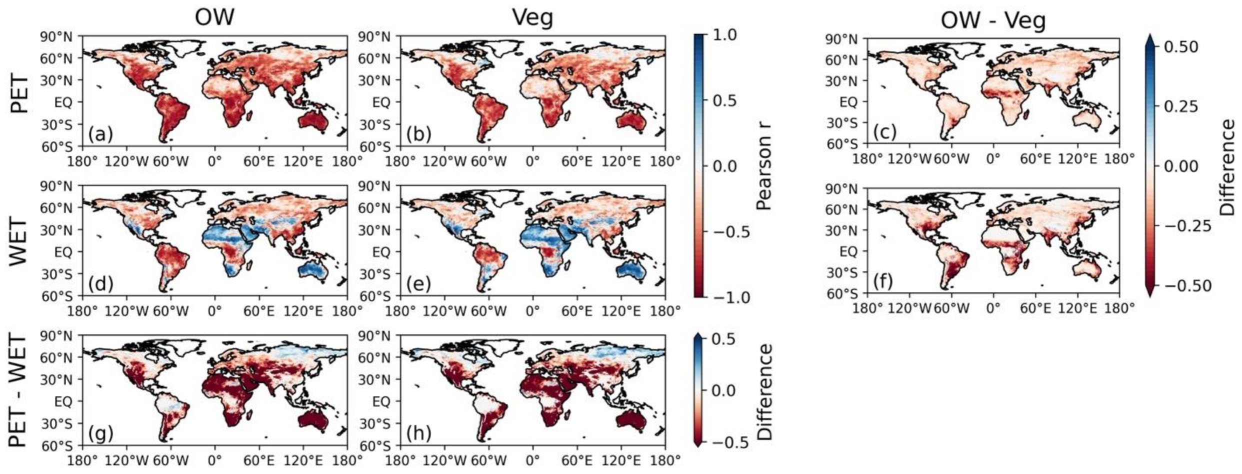

Fig. 2 Spatial distributions of the Pearson correlations (r) between annual P and evaporative demand estimates and their pairwise differences for 1985–2014. **a**,**b**, Correlations between P and PET_{OW}, and between P and PET_{Veg}, respectively. **c**, Differences r(P, PET_{OW}) – r(P, PET_{Veg}). **d,e**, Correlations between P and WET_{OW}, and between P and WET_{Veg}, respectively. **f**, Differences r(P, WET_{OW}) – r(P, WET_{Veg}). **g–h**, Changes in r due to feedback-driven inflation: r(P, PET_{OW}) – r(P, WET_{OW}) (g) and r(P, PET_{Veg}) – r(P, WET_{Veg}) (h).

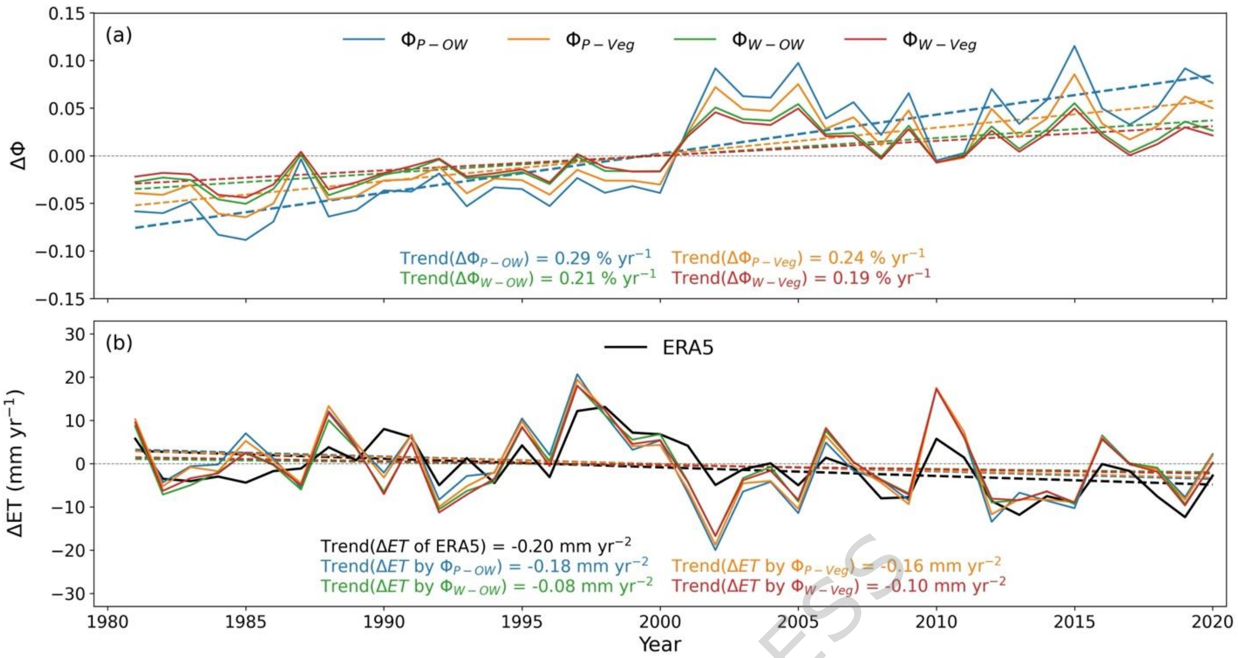

Fig. 3 Annual variations and long-term trends of global aridity index (Φ) and Budyko-framework E from the ERA5 forcing. **a**, Time series of global Φ anomalies (solid lines) relative to the 1985–2014 climatology, with the linear trends (dashed). **b**, Time series of Budyko-predicted global ET for each evaporative demand formulation alongside with ERA5 global E (black), with corresponding linear trends.

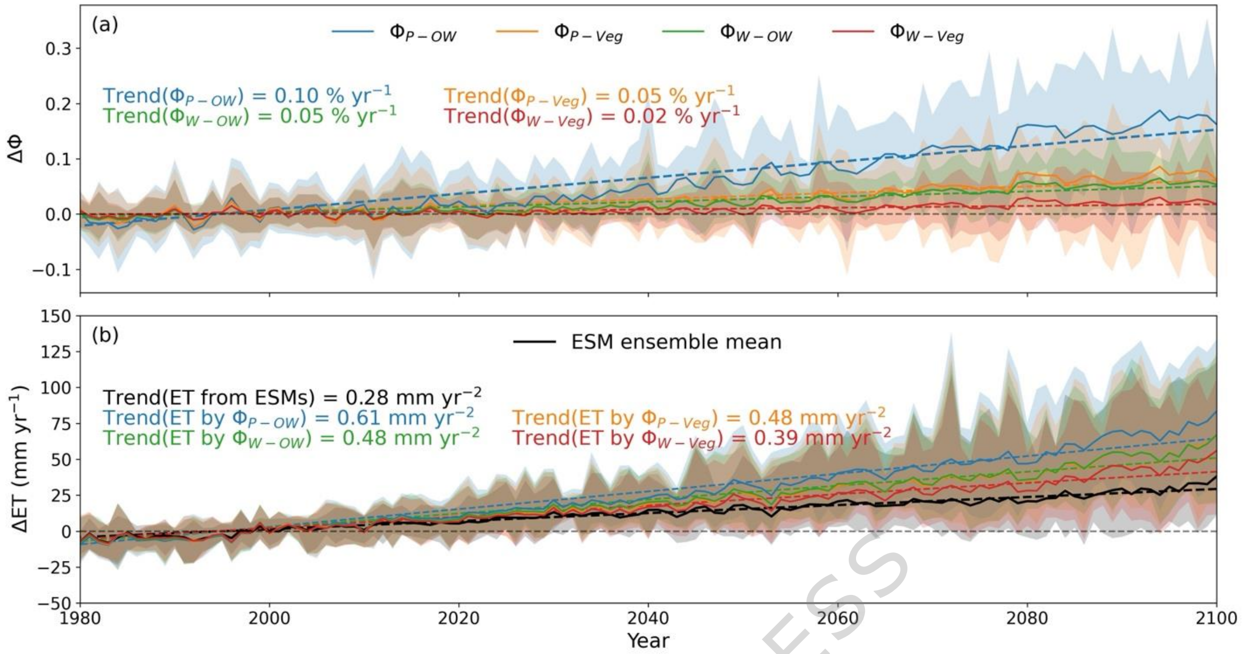

Fig. 4 Annual variations and long-term trends of global mean Φ and ET anomalies from the Budyko-framework and CMIP6 ESM projections. **a**, Global Φ anomalies (solid lines) relative to the 1985–2014 climatology, with ensemble mean linear trends (dashed). **b**, Budyko-framework-based global ET for each evaporative demand formulation and the multi-model ensemble ET (black), with respective linear trends (dashed lines). Shading shows the inter-model spread among ten CMIP6 models.